

8-1-2014

A Physically-Based Type II Supernova Feedback Model in SPH Simulations

Keita Todoroki

University of Nevada, Las Vegas, todoroki@unlv.nevada.edu

Follow this and additional works at: <https://digitalscholarship.unlv.edu/thesesdissertations>



Part of the [External Galaxies Commons](#), and the [Physics Commons](#)

Repository Citation

Todoroki, Keita, "A Physically-Based Type II Supernova Feedback Model in SPH Simulations" (2014). *UNLV Theses, Dissertations, Professional Papers, and Capstones*. 2219.

<https://digitalscholarship.unlv.edu/thesesdissertations/2219>

This Thesis is protected by copyright and/or related rights. It has been brought to you by Digital Scholarship@UNLV with permission from the rights-holder(s). You are free to use this Thesis in any way that is permitted by the copyright and related rights legislation that applies to your use. For other uses you need to obtain permission from the rights-holder(s) directly, unless additional rights are indicated by a Creative Commons license in the record and/or on the work itself.

This Thesis has been accepted for inclusion in UNLV Theses, Dissertations, Professional Papers, and Capstones by an authorized administrator of Digital Scholarship@UNLV. For more information, please contact digitalscholarship@unlv.edu.

A PHYSICALLY-BASED TYPE II SUPERNOVA FEEDBACK MODEL
IN SPH SIMULATIONS

By

Keita Todoroki

Bachelor of Arts in Physics
University of Hawai'i at Manoa
2011

A thesis submitted in partial fulfillment
of the requirements for the

Master of Science - Astronomy

Department of Physics and Astronomy
College of Sciences
The Graduate College

University of Nevada, Las Vegas
August 2014

Copyright by Keita Todoroki, 2014
All Rights Reserved



THE GRADUATE COLLEGE

We recommend the thesis prepared under our supervision by

Keita Todoroki

entitled

A Physically-Based Type II Supernova Feedback Model in SPH Simulations

is approved in partial fulfillment of the requirements for the degree of

Master of Science - Astronomy
Department of Physics and Astronomy

Kentaro Nagamine, Ph.D., Committee Chair

Stephen Lepp, Ph.D., Committee Member

Daniel Proga, Ph.D., Committee Member

Balakrishnan Naduvalath, Ph.D., Graduate College Representative

Kathryn Hausbeck Korgan, Ph.D., Interim Dean of the Graduate College

August 2014

ABSTRACT

A Physically-based Type II Supernova Feedback Model in SPH Simulations

by

Keita Todoroki

Dr. Kentaro Nagamine, Examination Committee Chair
Professor of Astronomy
University of Nevada, Las Vegas

We implement and test a core-collapse Type II SN feedback that is physically motivated and produces good agreement with observations in galaxy formation simulations. The model includes both kinetic and thermal feedback, allowing wind particles to receive a velocity kick that mimics galactic winds and distributes mass and metallicity to the interstellar and intergalactic medium. We also include a phenomenological stellar feedback to study a possible enhancement of the efficiency of the SN-II feedback by creating lower-density ambient gas medium of the stellar populations by distribution of thermal energy. Our SN-II model is unique in the sense that it computes the wind velocity and the lifetime of a supernova remnant by considering its evolution with the Sedov-Taylor solution rather than taking them as constant values. We find that by combining SN-II and stellar feedback the model alleviates overcooling and missing satellites problems. The model also produces outflows without a need for turning off hydrodynamical interactions, cooling and star formation by hand. Our preliminary results with cosmological zoom-in simulations imply the new model successfully reproduces the stellar-to-halo mass ratio. We conclude that the Sedov-Taylor solution can be used to reasonably approximate the physical properties and evolutionary time scales of supernova remnants in the galaxy formation numerical simulations.

ACKNOWLEDGMENTS

I would like to express my gratitude to my adviser, Dr. Kentaro Nagamine, for his advise and providing me valuable opportunities to work with him and some of the frontiers in the subject of galaxy formation simulations. I sincerely appreciate your understanding and patience to have me as your student who did not know anything about astronomy and computational astrophysics when I entered the program. I am also grateful to my committee members, Dr. Stephen Lepp, Dr. Daniel Proga and Dr. Balakrishnan Naduvalath for their helpful comments on my work.

If I were to acknowledge a person who has been a tremendous help on my research work, it is Dr. Robert Thompson without doubt. It has been a pleasure to have you as a colleague, and your feedback comments and supports on technical aspects made a lot of things possible. Thank you, Robert.

Finally, I am particularly grateful to Dr. Raja Almukahhal. I will never be able to thank you enough for your mentorship and friendship. I met you for the first time as an undergraduate, grading your students' homework during your brief stay at the University of Hawai'i at Manoa. After two weeks you eventually convinced me to pursue my academic career for a higher degree. It was the summer of 2011 and one of the best times of my entire life. Your constant care and guidance throughout my graduate studies at UNLV have given me a sense of reassurance, and I feel especially honored by your close friendship. You are like my father in the U.S., and I am looking forward to showing you how much further I can go.

TABLE OF CONTENTS

ABSTRACT	iii
ACKNOWLEDGMENTS	iv
LIST OF TABLES	vii
LIST OF FIGURES	viii
LIST OF SYMBOLS	ix
CHAPTER 1 INTRODUCTION	1
Overview	1
Type II Supernova	2
CHAPTER 2 EVOLUTION OF AN SNR	6
Explosion & energy transport mechanisms	6
Free expansion phase	7
Sedov-Taylor phase	8
Snowplow phase & fade away	10
CHAPTER 3 NUMERICAL METHODS	11
Motivations	11
SN-II feedback	13
<i>Energy, mass & metallicity distribution</i>	13
<i>Sedov-Taylor solution</i>	14
<i>Outflows</i>	16
<i>Eliminating unphysical adjustments</i>	16
Stellar feedback	17
Star formation prescription	18
CHAPTER 4 COMPUTATIONAL SETUP	19
CHAPTER 5 TEST RESULTS WITH ISOLATED GALAXY SIMULATIONS .	20
Feedback efficiency	20
Star formation history	20
Outflow rate & mass loading efficiency	21
Phase diagram	23
Computed variables for the SN-II model	23
Resolution dependency	24
CHAPTER 6 PRELIMINARY TEST RESULTS WITH COSMOLOGICAL ZOOM- IN SIMULATIONS	26
Setup	26
Stellar-to-halo mass ratio	26

CHAPTER 7 DISCUSSION & CONCLUSIONS	28
Future work	30
CHAPTER 8 AGORA COMPARISON PROJECT	33
Simulation setup	33
Overall results	34
Density projection	34
Density profile	35
Discussion	35
REFERENCES	47
CURRICULUM VITAE	50

LIST OF TABLES

Table 1	Disk parameters of the common IC for the idealized isolated galaxy	36
Table 2	Feedback efficiency parameters for tested cases	36
Table 3	Parameters for dark matter-only <i>AGORA</i> simulations	37

LIST OF FIGURES

Figure 1	A schematic evolutionary phases of SNR	38
Figure 2	A schematic representation of the SN-II feedback model for the SPH code	39
Figure 3	Star formation history of the tested cases for the isolated galaxy simulations compared	40
Figure 4	Outflow rates (dM/dt) and mass loading efficiency (η) compared . .	41
Figure 5	Projected gas density for the isolated disk galaxy simulations	41
Figure 6	Temperature variations in the gas mass for the isolated galaxy sim- ulations at $t = 1$ Gyr	42
Figure 7	Computed variables for SNII feedback	42
Figure 8	Resolution dependency test: star formation histories	43
Figure 9	Resolution dependency test: phase diagram & fractional gas mass .	43
Figure 10	Resolution dependency test: visualization	44
Figure 11	Stellar-to-halo mass ratio compared for the cosmological zoom-in simulations at $z = 0$	44
Figure 12	Projected gas density in $L = 1$ Mpc/h for the zoom-in simulations at $z = 0$	45
Figure 13	Projected dark matter density at $z = 0$	45
Figure 14	Dark matter density profiles of the target halo at $z = 0$	46

LIST OF SYMBOLS

Frequently Used Abbreviations

Symbol	Definition
ϵ_{SFB}	stellar feedback efficiency
η	mass loading efficiency; $\dot{M}_{outflow}/\dot{M}_*$
AGN	active galactic nuclei
c_s	effective sound speed of the ambient gas
E_k	kinetic energy available from SN; $0.283E_0$
E_{th}	thermal energy available from SN; $0.717E_0$
E_0	total SNe energy in units of 10^{51} erg
IC	initial condition
IGM	intergalactic medium
IMF	initial mass function
ISM	interstellar medium
L_\odot	solar luminosity; 3.826×10^{33} erg s ⁻¹
M_\odot	solar mass; 1.989×10^{33} g
N_{nab}	number of neighboring gas
n_0	ambient gas density in cm ⁻³
R_s	radius of SNR
SH03SF	Springel & Hernquist (2003) star formation model
SF	star formation
SFB	stellar feedback
SFR	star formation rate
SN/SNe	supernova/supernovae
SNII	Type II supernova feedback model
SNIISFB	SNII and SFB both included case; suffixed integer indicates the strength of ϵ_{SFB}
SNR	supernova remnant
SN-Ia	Type Ia supernova
SN-II	Type II supernova
SPH	smoothed particle hydrodynamics
ST	Sedov-Taylor
t_*	star formation timescale
$t_{deposited}$	time at which SFB energy is deposited in the ambient gas
$t_{exploded}$	time at which star explode as SN
t_{fade}	time at which an SNR fades away and dissipates
t_{rad}/t_{ST}	end of ST phase when radiative loss becomes non-negligible
WINDS	strong wind model from Springel & Hernquist (2003)

CHAPTER 1

INTRODUCTION

Overview

The complete theoretical understanding of the galaxy formation and evolution remains a challenge even with the improved numerical techniques, the increased availability of large computational resources and implications from observational evidence. The difficulties mainly stem from the fact that we still have observational constraints and lack of understanding of the detailed physical processes that affect galaxy formation and evolution in cosmic time scale. Meanwhile, the apparent success of the Λ CDM model tested on cosmological simulations in reproducing the dark-matter density and velocity distributions clearly demonstrates the validity of the cosmological models (e.g. Katz et al., 1996; Weinberg et al., 2002; Springel et al., 2006). Despite of the success, however, there is still a great deal of uncertainties in the baryonic evolution, and that the detailed numerical implementations of the physical processes must be examined with caution. In particular, in the past decades the discrepancies seen in theoretical predictions and observations raised awareness of accurately integrating small-scaled physical processes. Some of the important discrepancies seen are (1) the excessive star formation due to *overcooling problem* in simulations (White & Frenk, 1991; Balogh et al., 2001; Kereš et al., 2009) (see the detailed discussion in § 3), (2) overprediction of the low-mass and high-mass objects in the galaxy luminosity function by simulations (Silk et al., 2013), and (3) a larger number of small satellite galaxies produced by simulations (*missing satellites problem*) (see § 6) (Klypin et al., 1999; Moore et al., 1999).

The discrepancies can be largely attributed to inappropriately overlooked or inaccurately implemented feedback mechanisms from a variety of origins, such as supernovae (SNe), photoionization, stellar winds and AGN. Studies show, for ex-

ample, that SNe and active galactic nuclei (AGN) feedback are energetically important in reproducing observed galaxy properties. They are able to resolve the discrepancies in the low-mass and high-mass ends of the galaxy luminosity function, respectively, by means of suppressing the star formation rate in numerical simulations (see a review paper on galaxy formation by Silk et al. (2013)). Thus proper treatments of the baryonic physics are required to bridge the gap between theories and observations.

In galaxy formation hydrodynamical simulations, however, we have resolution limits that constrain us from how the physics can be implemented. For this reason, previous studies have used phenomenological models and implemented SN feedback as a sub-grid model to simulate galaxy formation and evolution. In this work, we are thereby motivated to test a physically-based supernova Type II (SN-II) feedback as a progressing step toward studying the complete picture of the galaxy formation and evolution. We study its effect on suppressing the excessive star formation by overcoming the over-cooling problem that is notably seen in numerical simulations from two perspectives: by means of producing outflows via kinetic feedback and by heating up the ambient gas via thermal feedback. Our main goal here is to implement a SN-II feedback that does not depend largely on phenomenological methods.

Type II Supernova

Evolving stars end their lives in various ways. Each scenario played for a stellar death is primarily determined by their physical properties, or to be specific, their initial masses. For instance, stars with masses $> 8 M_{\odot}$ are thought to end their lives by core-collapsing due to their large masses. The types of the systems, i.e. whether it is a single/binary system, in which the star resides is also a key determinant of the outcome of the stellar death (see Chapter 2 for more in depth discussion on

the physical processes of the stellar death). Supernovae is a general term used by astronomers for explosive stellar death events releasing energy up to $\sim 10^{51} - 10^{52}$ erg with luminosities of $\sim 10^9 - 10^{10} L_{\odot}$. This large energy budget sets supernovae apart from less energetic novae, as the name implies. Therefore, the significance of studying supernovae comes from the possible impact on the galaxy formation and evolution, which eventually is tied into a much larger scale of structure formation.

Supernovae are generally subdivided into classes based on their emission spectra and light curves. The two largest known classes are Type I and Type II, and that they are categorized based on the absence/presence of hydrogen line in the spectra, respectively. The spectra used to classify the types of supernovae are typically observed from the supernova remnant as a result of the interactions between the supernova ejecta and the ambient gas medium. The conversion of kinetic energy released by supernova into thermal energy leads to ionization of the surrounding gas; thus the kinds of spectra seen are a function of temperature. In the meantime, the chemical composition of the stars at the time of explosion, which is largely determined by their initial masses, is yet another important factor that governs the types of spectra we can observe. The presence of hydrogen line that characterizes Type II supernovae is a good indicator of the hydrogen shell that enclosed the exploding stars. Importantly, the light curve, which tells us the change of the supernova luminosity as a function of time, is also examined to further classify Type II supernovae. Type II-P and II-L, for example, are known to show a plateau and monotonically declining light curves, respectively.

Because nothing is wasted in this universe, exploded stars contribute to the universal baryonic recycling mechanism by distributing their masses into the interstellar and intergalactic medium (ISM & IGM). It is believed that the observed metallicities in the ISM and IGM are partly delivered from supernovae by outflows, and that those metals can be recycled to form other stars. Therefore, in a broad sense su-

pernovae self-regulate the star formation. This self-regulating mechanism should thus be considered as one of the fundamental mechanisms that controls the galaxy formation and evolution. Accumulating observational evidence shows that supernova explosions remain highly influential to the surrounding medium well over thousands of years as supernova remnants (SNRs).

This accentuates the importance of accurately modeling supernovae and SNRs when galaxy formation and evolution are studied in numerical simulations. The detailed theoretical understanding of supernovae is still incomplete, and the complex interplay between the stellar evolutionary processes and the variabilities of the ambient gas medium has been an impediment to elucidating the complete picture. Even with a solid theoretical understanding, modeling a supernova mechanism in galaxy formation simulations to study the large-scale structure evolution over the cosmic time requires to overcome the computational constraints without compromising too much of the theoretical foundations. Previous models implemented and used in a rather phenomenological manner might be useful in studying the larger scale impact on the galaxy formation and evolution. However, with improved computational resources and numerical techniques, it has become possible to model a supernova mechanism with a finer physics to mimic some of the key evolutionary stages of supernovae/SNRs. Consequently, the primary motivation of this work is rooted strongly in the improvement of the overall physical processes of a supernova mechanism in hopes of elevating the predictive power of galaxy formation numerical simulations.

This work is organized as follows. In Chapter 2, we describe the evolutionary processes of the SNR, starting from the free-expansion phase, Sedov-Taylor phase, snowplow phase and fadeaway. We then discuss the numerical methods and implementations in Chapter 3 and 4. Finally, we present our test results with isolated galaxy and cosmological zoom-in simulations in Chapter 5. We summarize our

findings and future work in Chapter 6. At the very end in Chapter 7, we additionally include a brief summary of the results from dark matter only simulations done as part of a collaboration project *AGORA*.

CHAPTER 2

EVOLUTION OF AN SNR

In this section, we review the outline of the evolution of a supernova remnant. A massive star ends its life as a core-collapse supernova, a violent explosion that leaves behind a neutron star or a black hole. The explosion subsequently creates a SNR that evolves into a hot bubble and deposits a large amount of energy into the ISM as it sweeps up the surrounding materials and expands into the ISM. The evolution of the SNR can generally be categorized into four phases – the free-expansion, Sedov-Taylor, snowplow and fadeaway phases (Figure 1).

Explosion & energy transport mechanisms

Once the core of a massive star exhausts the fuel for further nuclear reaction to counteract with gravity, the star begins to collapse in a dynamical time scale. During this process the iron core collapses nearly at a quarter of the speed of light and eventually shrinks down to a 10-km radius neutron star. The entire process is accompanied with the release of an explosive energy as well as the ejecta from the evolved star, which subsequently produces an SNR (e.g. see Woosley & Janka, 2005, and references therein).

In general, the conversion of the kinetic energy into heat drives the overall physical processes in the evolution of SNR. However, a complex interplay between different processes for the energy generation and transport mechanisms remains unclear. The favored mechanism suggests that the transport of a large fraction of the initial SN energy is done by neutrinos. They are produced by a process called *electron capture*, which destabilizes the iron core, and neutrinos carry away about 99% of the total energy released by a core collapse explosion (Haxton, 2000) via



In addition, Burrows et al. (2006) describe the essential role played by neutrinos in the SN explosion mechanism, where they delve into discussing the neutrino scattering and absorption as well.

Other possible explosion and energy transport mechanisms have also been proposed and studied in details. In particular, rapid rotation, magnetic fields and cosmic rays are some of the main physical features that characterize and affect the dynamical evolution of SNe (e.g. Burrows, 2013; Hanasz et al., 2013). The studies by Hanasz et al. (2013), for example, suggest that only 10% of SN energy as cosmic rays, neglecting the thermal and kinetic energy input, is capable of driving a large scale galactic wind in an environment similar to star-forming high-redshift galaxies. Their studies imply that these mechanisms are indeed playing key roles in carrying away the SN energy and could account for some of the observed features from SNe.

Free expansion phase

Cox (1993) argues that for a typical explosion in a uniform medium, an explosion is immediately followed by free expansion of the ejecta with a velocity much greater than the sound speed in the ambient medium due to the large density gradient (Figure 1). This results in a shock that is produced by the large release of energy from the core collapse, which converts the gravitational potential energy into heat in a free-fall time scale (the free-expansion phase). The shock heats up the interior and creates a low-density environment within the SNR as it propagates adiabatically with a decreasing velocity due to the deceleration caused by the ambient gas pressure and density. The adiabatic expansion is due to the initially much shorter sound-crossing time compared to the radiative cooling time. This free expansion phase usually lasts for $\leq 10^3$ years.

The typically assumed value for the energy released by a single core-collapse

SN explosion, E_0 , is 10^{51} erg, which comes from

$$E_0 = \frac{1}{2} M_{ej} v_{ej}^2 \quad (2.2)$$

with the assumed ejected mass M_{ej} to be $\sim 1 M_\odot$ ($\sim 2 \times 10^{33}$ g) and the initial speed of the ejecta v_{ej} to be $\sim 10^4$ km s $^{-1}$. In reality, however, the explosion energy varies and could be a function of progenitor mass, rotation rate, magnetic fields, metallicity and possibly other factors might also be involved, such as the properties of the residual compact object (Burrows, 2013). In fact, Rest et al. (2011) finds that a highly luminous core-collapse SN 2000ma could have its explosion energy greater than 10^{52} erg.

Once the pressure of the shocked circumstellar medium exceeds that of the thermal pressure of the SNR during the free expansion phase, a reverse shock is produced. The reverse shock propagates inward and re-heats the SNR, which has been adiabatically cooled since the explosion, and the outward propagating shock still continues to expand. The free expansion phase ends when the reverse shock reaches the center of the explosion. Thus the reheating within the SNR is complete and it is entirely thermalized. This is also when the expansion rate of SNR starts to slow down by entering a adiabatic phase called the Sedov-Taylor phase.

Sedov-Taylor phase

By the time the reverse shock reaches the center of the explosion, the evolution of a SNR can now be approximated by the Sedov-Taylor (ST) solution (e.g. Sedov, 1959; Taylor, 1950; Cox, 1972, 1993, and references therein), which was independently discovered by a British scientist Geoffrey Taylor and Leonid Sedov of the Soviet Union in their studies of the effect of nuclear explosions (Figure 1). It assumes a point explosion with a negligible ejecta mass and the uniform ambient

gas density. The energy release is also assumed to be done instantaneously. The radiative cooling during the ST phase is neglected because the cooling rate from adiabatic expansion is faster than that of from radiation in the hot and low density SNR. The other neglected factors in this model are the pressure from the ambient medium and the magnetic field. As the SN blastwave evolves, it can be well approximated by the ST solution until the temperature of the shock drops to the point where the radiative cooling becomes important. Note that the approximation of a point explosion is reasonably well only when the mass that is swept up by the outward propagating shock wave greatly exceeds the mass of the initial ejecta (Shu, 1992). The approximation, therefore, becomes better as the swept-up mass increases in later times of the phase.

It is approximated that this adiabatically expanding phase ends when the shock propagation is decelerated to the point where the cooling rate by radiation behind the shock becomes non-negligible compared to that of adiabatic expansion. This occurs approximately when the fractional energy loss reaches a third of the initial energy. From this argument Draine (2011) derives the following relationships at the time of the end of the ST phase:

$$v_s = 188 \left(\frac{E_k}{n_0^2} \right)^{0.07} \text{ [km s}^{-1}\text{]}, \quad (2.3)$$

$$R_s = R_{SNR} = 23.7 E_0^{0.29} n_0^{-0.42} \text{ [pc]}, \quad (2.4)$$

$$t_{rad} = t_{End\ of\ ST\ phase} = 49.3 \times 10^3 E_0^{0.22} n_0^{-0.55} \text{ [yr]}, \quad (2.5)$$

where R_s is the radius of the SNR, E_0 is the total SNe energy in units of 10^{51} erg as a widely accepted canonical value, E_k is the kinetic energy from SNe which is equivalent to $0.283E_0$ (see § 3), and n_0 is the density of the ambient gas in cm^{-3} .

Snowplow phase & fade away

As the radiative cooling becomes important, the thermal energy of the swept-up material is rapidly radiated (Figure 1). Concurrently, the thin dense shell at the edge of the SNR further expands outward by its own momentum and partly by the remaining thermal pressure. The cooling lowers the pressure behind the shock, and the shock velocity continues to decrease as the dense expanding shell gains and carries away more material from the surrounding medium. The SNR eventually begins to fade away and merges into the ISM as the shock front velocity is reduced to the effective sound speed of the ambient gas medium. This occurs roughly when the pressure of the shock front equals that of the ambient medium. Following Draine (2011), fade away time, t_{fade} , is then approximated to be

$$t_{fade} \approx 1.87 \times 10^6 E_0^{0.32} n_0^{-0.37} \left(\frac{c_s}{10 \text{ km s}^{-1}} \right)^{-\frac{7}{5}} \text{ [years]}, \quad (2.6)$$

where c_s is the effective sound speed in the ambient gas. This marks the end of a SNR and it dissipates into the ISM.

CHAPTER 3

NUMERICAL METHODS

Motivations

A mounting evidence suggests that the energetic feedback processes such as SNe and AGN are essential in explaining the galaxy formation and evolution. A number of different SN feedback models has been proposed and studied in literature, and the detailed implementations vary from code to code. The main obstacle in implementing these models is the limit set by the numerical resolution. The subgrid models have therefore been the mainstream in the past decade and used to mimic the observational phenomena in order to accommodate the inability of galaxy-scale hydrodynamic simulations to accurately capture the small-scale dynamics.

An important progress has been made to alleviate this resolution problem by cosmological *zoom-in* simulations. This 'zoom-in' technique allows us to study a particular region of interest in a cosmological scale with a finer resolution. The advantage is that it is computationally less expensive and a galaxy of interest can be studied with higher resolution compared to the traditional cosmological simulations. The *MUSIC* code by Hahn & Abel (2011) can be used to create an IC for zoom-in simulations in such a way that one can specify the desired resolution and box size. With zoom-in simulations, we can therefore test our feedback model for its validity in smaller-scale, namely sub-kpc regime, by resolving finer physics that is implemented. In particular, the cosmological zoom-in simulation time step can now be comparable to or less than the life time of a SNR. This in turn allows us to model and test a SN feedback that tracks the approximated evolutionary phases of SNR instead of an entirely phenomenological feedback.

In addition to the resolution issue, observations demand those models to suf-

ficiently regulate the overly produced stellar mass in simulations. The so-called *overcooling* problem arises because when the thermal energy from the SN/stellar feedback is deposited into the high-density star-forming regions, the cooling time scale becomes short and the deposited thermal energy is quickly radiated away, resulting in an overproduction of stars compared to observational expectations. To circumvent this problem many works utilize kinetic feedback as a more efficient method to transfer energy (via momentum injection) without suffering from the radiative loss seen in a thermal feedback (e.g. Kay et al., 2002; Springel & Hernquist, 2003; Oppenheimer & Davé, 2006; Dalla Vecchia & Schaye, 2008; Dubois & Teyssier, 2008; Choi & Nagamine, 2011; Durier & Dalla Vecchia, 2012; Agertz et al., 2013; Hopkins et al., 2013). Kinetic feedback generally refers to a mechanism that gives kinetic energy into the star's neighboring gas particles as in a form of velocity kick. A very important consequence of this type of feedback mechanism is that the energy along with mass and metals can be carried away with galactic outflows and could account for the gas recycling mechanism in the ISM and IGM.

Our primary goal is to test an SN feedback model that is as physically motivated as possible rather than relying on phenomenological approach that has commonly been used in the previous works. We model the feedback based on the evolutionary process of the SNR and use the ST solution for quantifying the physical properties of the conglomeration of SNRs in our SPH code. A single SN event and the subsequent SNR evolution cannot be resolved in our current simulations. However, the cumulative effect of SNe can be reasonably modeled and it is capable of reproducing some of the main features we see in observations. Furthermore, by making the feedback more physically-based, the number of tunable parameters can be preferably reduced at the same time. The recent improvements on the numerical techniques, such as the zoom-in simulations mentioned in this section, have made it possible to achieve our goal of making the feedback mechanisms more physically-

based by resolving finer scale physics.

SN-II feedback

Energy, mass & metallicity distribution

In our SPH code, a single star particle represents a stellar population. Therefore, the total energy from multiple SNe by a single stellar population must be calculated by the initial mass function (IMF). We follow Kim et al. (2014) and use a Chabrier (2003) IMF to calculate the total energy and number of SNe explosions, assuming stars with $8 - 40 M_{\odot}$ undergo core-collapse SNe (which would include Type II, Ib and Ic), and use 10^{51} erg/SN as the fixed value. We also assume that the IMF is universal and remains unchanged in the cosmic time scale. The total SNe energy produced by a stellar population is then distributed among the star's neighboring gas particles. We adopt Durrer & Dalla Vecchia (2012)'s work and use 71.7% as the thermal and 28.3% as the kinetic energy based on the energy conservation. The energy deposition is completed in a single time step, which is also applied in Dalla Vecchia & Schaye (2012).

Additionally, we include the mass return and metal production from the core-collapse SNe by following the criteria described in the *AGORA* project (Kim et al., 2014). The mass return (R) from stars with $8 M_{\odot} < m < 40 M_{\odot}$ leaves behind a remnant of $w_m = 1.4 M_{\odot}$, and it follows

$$R = \int_{8M_{\odot}}^{40M_{\odot}} (m - w_m) \phi(m) dm, \quad (3.1)$$

where $\phi(m) = dn/dm \propto m^{-2.3}$ for core-collapse SNe with a Chabrier IMF. For metal production from core-collapse SNe, we compute the produced metallicity mass in

terms of Oxygen and Iron as

$$M_Z = 2.09M_O + 1.06M_{Fe}, \quad (3.2)$$

with the corresponding fractional masses of the two species to be $0.0133/M_\odot$ and $0.011/M_\odot$, respectively. They are distributed in exactly the same manner as the SNe energy.

In the SPH code, the surrounding mass density, ρ , of an SPH particle is computed by the mass-weighted smoothing kernel by

$$\rho_i = \sum_{j=1}^{N_{ngb}} m_j W(|\mathbf{r}_{ij}, \mathbf{h}_i|), \quad (3.3)$$

where $\mathbf{r}_{ij} \equiv \mathbf{r}_i - \mathbf{r}_j$, N_{ngb} is the number of neighboring gas particles, m is the particle mass, W is the smoothing kernel function, and h is the particle softening length (see Springel, 2005). N_{ngb} is specified in the param file, in which our model uses 128 ± 2 . We then use R_{SNR} (Equation 2.4) to find the neighboring gas particles that are influenced by the SNII feedback.

The fraction of kinetic & thermal energy, mass return, and metals that each Ngb gas receives is calculated by mass-weighted formula

$$\Delta A_i = \frac{m_i W(|r_i - r_s|, h_s)}{\sum_{j=1}^N m_j W(|r_j - r_s|, h_s)} A, \quad (3.4)$$

where A can be any of those four quantities (Stinson et al., 2006).

Sedov-Taylor solution

It is a common practice in some feedback models of galaxy formation simulations to use a fixed, constant wind velocity that is motivated by observations (e.g. Springel & Hernquist, 2003). However, the shock front velocity can be calculated

by the ST solution as seen in Equation (2.3), which depends only on two physical parameters, the initial SN energy, E_0 , and the ambient gas density, n_0 . The dependency of the SNR's properties on n_0 is well-established that the exploding stars' surrounding environment largely affects the morphology and spectral line emissions of the SNR (Osterbrock & Ferland, 2006). Although we cannot resolve the detailed SNR properties in sub-pc scale, the ST solution can mimic the ambient gas density dependent nature of the SNR. Importantly, Equation (2.3) & Equation (2.4) clearly shows that the blast wave propagates at a larger velocity and the SNR can expand to a larger distance in a diffuse environment, whereas in a dense medium the opposite is true. Overall, the application of the ST solution adds more physically-based features to the SN feedback and reduces the number of free parameters.

We take 28.3% of the total SNe energy ($E_k = 0.283E_0$) as kinetic energy available for computing the wind velocities by using Equation (2.3). Note however that the influence of SNII radius (R_{SNR}), the time at which ST phase ends (t_{rad}), the fade away time (t_{fade}) are calculated based on the *entire* SNe energy (E_0) instead of E_k . In our model, the ST solution (Equations (2.3) & (2.4)) are used to calculate the approximate SNR properties at the *end* of the ST phase. Equations (2.5) & (2.6) are then used to further approximate the times at which the ST phase ends and the SNR fades away, respectively, based on the current ambient gas density (n_0) and E_0 .

All the physical quantities of SNR calculated by the ST solution apply only for the case when the SNR is in the ST phase. Since the simulation time-step can be larger than the ST phase, it can be entirely skipped depending on the size of the time-step, which depends on the resolution: the higher the resolution, the smaller the time-step. It is also possible to express the shock velocity and the radius of the SNR as a function of time (i.e. the time elapsed since the SNe explosions). However, this adds a strong dependency on the resolution to the model, for the size of the

time-step can differ by orders of magnitude. To avoid this, the model approximates the physical properties of SNR at the end of the ST phase.

Outflows

We allow those kicked gas particles to receive more than one velocity kicks by other SN explosions. The randomly-oriented directions given to them produce outflows, and some of which form galactic fountains by falling onto the disk after the kick due to the greater escape velocity of the galaxy.

A potential drawback of this type of feedback is that if the number of the wind particles is only a few, it results in a less isotropic outflow as Dalla Vecchia & Schaye (2008) argue. However, owing to the fact that an SNR is not necessarily isotropic due to the variations in the surrounding gas density as observations from the X-ray and IR morphology of SNRs show (Lopez et al., 2013), non-isotropic outflows that might be produced in our model is justifiable.

Eliminating unphysical adjustments

Within a concept of testing a physically-based model, we also eliminate some artificial adjustments which have been notoriously done in previous works. We highlight that in this work the hydrodynamical interactions and radiative cooling are not artificially turned off by hand for a fixed period of time for the sole purpose of reproducing the desired results.

Turning the hydro interactions off is especially considered unphysical, and for a physically-based model it defeats the whole purpose. For example, a constant wind model employed by Springel & Hernquist (2003) produces bipolar galactic outflows as star formation takes place and heats the surrounding gas. In their model the hydro are turned off by hand for a certain period of time when the kicked particles are labeled as 'winds'. Although turning off the hydro helps to enhance producing

outflows and regulating star formation rate, it is done so artificially, based on a rather phenomenological perspective.

Note also that it is computationally less expensive to turn off hydro; for the case of the constant wind model turning hydro *on*, there is an 77% increase in CPU time compared to the case without hydro for the wind particles.

Within the framework of depicting the evolution of an SNR approximated by the ST solution, the ST phase is an adiabatically expanding phase and considered the radiative cooling has negligible effect. Hence it is physically reasonable to turn off radiative cooling for the gas in the ST phase, which typically lasts 0.1 Myr before moving on to the snowplow phase where the radiative cooling should now become non-negligible. Note that in previous models studied by others (e.g. Stinson et al., 2006) turn off cooling for a much longer time scale, such as 30 Myr. This time scale accounts roughly for a fadeaway time for an SNR. We find that the calculated time for a typical ST phase is in the order of 10^5 years, and therefore turning off radiative cooling for $\sim 10^7$ years is an overkill (see Figure 7 and § 5 for detailed discussion).

Stellar feedback

In this work we study how the effectiveness of the SN-II feedback changes with or without stellar feedback (SFB). In contrast to a physically-based SN-II feedback, we use a modified version of a phenomenological SFB model from Stinson et al. (2013). This model utilizes a luminosity-mass relations from binary star systems, and the converted energy is deposited among the neighbors as in a form of pure thermal energy. Our SFB model, however, does not artificially turn off the radiative cooling for a certain period of time unlike their model (= 30 Myr) as we criticized. We test early stellar feedback efficiencies ϵ_{SFB} of 10, 20 and 30% to study the overall effect of the additional thermal feedback to the SN-II feedback on the galaxy properties.

In some literature the thermal energy from SFB is distributed gradually in an exponential decay rate. In this work we simply dump the thermal energy at a constant rate until $t \geq t_{\text{explode}} = 4 \text{ Myr}$. The fractional thermal energy (ΔE_{th}) from a star particle for SFB in a single time-step is

$$\Delta E_{th} = \epsilon_{SFB} E_0 \frac{t - t_{\text{deposited}}}{t_{\text{explode}}}, \quad (3.5)$$

where t is the current time, $t_{\text{deposited}}$ is the time at which the star deposited a fraction of the thermal energy in the previous time-step. ΔE_{th} is then distributed among all the neighboring gas particles using Equation (3.4).

Star formation prescription

We use a modified version of SF model originally developed by Springel & Hernquist (2003) (hereafter SH03SF model). SH03SF model treats the ISM as a spatially averaged multi-phase medium composed of cold and hot clouds, represented by each SPH particle. Conversion of cold clouds results in star formation, and it is followed by:

$$\dot{\rho}_* = (1 - \beta) \frac{\rho_c}{t_*}, \quad (3.6)$$

where SFR is described by β , a mass fraction of short-lived massive stars that are assumed to instantaneously explode as supernovae, ρ_c the density of cold clouds, and t_* the star formation timescale that is proportional to $(\rho/\rho_{th})^{-1/2}$ with total gas density $\rho (= \rho_{hot} + \rho_c)$ and the threshold gas density ρ_{th} .

Because the SN-II feedback separately treats SN explosions 4 Myr after the star formation, we modify the SH03SF model so that there is no dependency on β in the star formation criteria. Furthermore, the imposition of equation of state for the star forming gas done by the instantaneously exploding SNe is disabled when SNII or SFB are used.

CHAPTER 4

COMPUTATIONAL SETUP

We use a modified version of the smoothed particle hydrodynamics (SPH) code GADGET-3 (originally described in Springel 2005). Our conventional code includes radiative cooling by H, He, and metals (Choi & Nagamine, 2009), heating by a uniform UV background radiation of a modified Haardt & Madau (1996) spectrum (Katz et al., 1996), star formation, supernova feedback (previous model), the Multi-component Variable Velocity (MVV) wind model (Choi & Nagamine, 2011), a sub-resolution model of multi-phase ISM (Springel & Hernquist, 2003), a density independent SPH (DISPH) (Hopkins, 2013; Saitoh & Makino, 2013), a time-step limiter (Saitoh & Makino, 2009) and a quintic spline kernel (Morris, 1996).

We test our model with an isolated galaxy first to study the sub-kpc scale behaviors of the feedback before moving on to testing it with cosmological zoom-in simulations. We use common initial conditions for an idealized, Milky Way-like isolated galaxy provided by the project *AGORA* (Kim et al., 2014) (credits to Oscar Agertz) for testing our model with isolated galaxy simulations. The disk properties are summarized in Table 1. With the common initial conditions, our work should alleviate possible difficulties in comparison among other models with other codes later on. For the setting used for the preliminary testing with cosmological zoom-in simulations, please refer to § 6.

CHAPTER 5

TEST RESULTS WITH ISOLATED GALAXY SIMULATIONS

Feedback efficiency

Table 2 presents the symbols for various cases tested with isolated galaxy. We tested cases with a combination of SN-II and stellar feedback (SFB) as well as cases with only each of the feedback alone to study their relative contributions to the overall feedback efficiency. We limit our case studies as follows: all the SN-II feedback takes the canonical value of 10^{51} erg per SN event that is distributed among the neighboring gas; SFB is tested with the stellar feedback efficiency (ϵ_{SFB}) of 0.1 (or 10% efficiency), 0.2 and 0.3.

Star formation history

Regulating star formation rate (SFR) is one of the key aspects of what an effective feedback is expected to accomplish in galaxy formation simulations. In particular, so-called *over-cooling* problem must be overcome in order for the simulations to be able to produce galaxies with stellar-to-halo mass ratio that is in agreement with observations. This generally requires suppression of star formation rate in the early times and subsequently preventing galaxies from accumulating excessive stellar mass compared to observational expectations.

Figure 3 compares star formation history of the tested cases. As it is clear from the figure, SNII alone can significantly regulate the SFR, whereas SFB by itself is less efficient even with the increased efficiencies. This is highlighted by the SFRs for SNIISFB, SNIISFB2 and SNIISFB3 where the overall SFR is not largely affected by the inclusion of SFB, except for SNIISFB3 which shows a slightly stronger suppression of SFR.

It is important to note that SFB can also *enhance* the SFR as seen in the increased

SFR in the early times. This is likely due to the formation of dense gas regions as a result of the swept up gas by SFB. Unlike SNII in which the deposition of thermal energy is done in a single time-step, SFB does it over multiple time-steps if the simulation time-steps are shorter than 4 Myr. This creates low-dense gas regions in the immediate vicinity of the star, while forming denser regions on the outskirts.

For comparison we included the results from previous models, namely SH03SF model and a constant wind model (WINDS). The SH03SF model deposits SNe energy instantaneously immediately after the star formation so that the suppression of SFR in the earlier time is stronger compared to the SFB. The key improvement of SNII over WINDS is that the very similar degree of regulation of the SFR is achieved by SNII without the need of artificially turning off the hydrodynamical interactions for the wind particles. Furthermore, SNII computes the wind velocity for individual gas particle by the ST solution that depends on the ambient gas density and the SN energy rather than assigning a fixed wind velocity that is dependent on free parameters as in WINDS. SNII, therefore, has an advantage over WINDS by being more physically-based and regulating the SFR to the same degree at the same time.

Overall, Figure 3 stresses the clear advantage of the kinetic feedback over the thermal feedback in regulating SFR. The thermal feedback alone has been proven to be inefficient in previous works in literature, and our results show the general agreement with this.

Outflow rate & mass loading efficiency

In WINDS and MVV models, the mass loading efficiency (η) is either set to a constant value or calculated based on the velocity dispersion of the host galaxy, respectively. SNII, on the other hand, does not use η as a parameter so that it is directly computed from the outflow rate and SFR. Figure 4 compares the outflow rate and η for selected cases at $t = 1$ Gyr.

By comparing SNII and SNIISFB, there is only a minor difference in both outflow rate and η , as expected from their SFRs. The higher outflow rate and η for SNIISFB3 are also naturally expected because of its lower SFR. The steady decrease and increase in the outflow rates and η , respectively, of SNII, SNIISFB and SNIISFB3 are well correlated with the equally steady decrease in their SFRs due to the depletion of the gas reservoir. Note that for isolated galaxy simulations we do not have mergers, and thus the outflows and the conversion of gas into stars keep reducing the total gas mass available for further star formation on the disk.

The primary reason for the stronger outflow rate and the higher η for the WINDS model is the artificial turning off of the hydrodynamical interactions for the wind particles. We find that the strength of the outflow is dramatically reduced when the hydrodynamical interactions are turned on for WINDS. This also helps the outflow at 5 kpc from the disk plane to remain as strong as that of at 3 kpc for WINDS.

As such, Figure 4 clearly shows the significance of the hydrodynamical interactions, which further emphasizes that artificially turning it off is not only unphysical but also unreasonable. Although our SNII model has a weaker η , which ranges 2 \sim 3, as opposed to that of WINDS (5 \sim 6), SNII is capable of regulating the SFR equally strong as WINDS.

We compute the outflow rate as

$$\dot{M} = \sum_{i=1}^N \left(\frac{M_i v_i}{\frac{4}{3} h_i} - \frac{M_i v_i |z_{plane} - z_i|^2}{\frac{4}{3} h_i^3} \right), \quad (5.1)$$

where i denotes the i_{th} gas particle that is *touching* the z -plane; i.e. if the plane is within the smoothing length of the gas particle h_i and its velocity vector in the z -direction is > 0 , then the particle is considered outflowing. M_i is the mass, v_i is the velocity, and z_i is the z -position of the i_{th} gas particle.

Phase diagram

Figure 6 presents the phase diagram for selected cases. It is instructive to first compare SNII & SFB. The primary effect of the deposition of thermal energy over multiple time-steps by SFB (whereas SNII does it in a single time-step) is that the star's neighboring gas particles are constantly swept up and form less densely populated regions (see also Figure 5). However, the feedback effect from SFB is relatively weak so that the large less dense regions shown by Figure 5 is mostly due to the intense consumption of gas by excessive star formation. The inefficiency of SFB is also clearly seen in the larger cold gas mass in the dense gas regions with $\log n_{gas} = -2$ to 0. This makes the disk largely dominated by cold gas and fails to capture the multiphase nature of the ISM, which would further make it prone to excessive star formation.

Comparing SNII and SNIISFB, there is only a minor difference, although slightly more fractional cold gas is converted to warm gas in SNIISFB due to the additional thermal feedback by SFB. The extended tail seen in SNII and SNIISFB in the low density region is caused by the outflows from SNII feedback, which are strong enough to kick the gas to non-star-forming regions. Because the young stars mainly form in the disk spirals, the kicked gas become free from SNII and SFB once they escape the galactic potential well. The direct result is the production of outflows. These outflows eventually cool down to a lower temperature by adiabatic expansion. Note that since we do not have molecular cooling implemented in the code, the gas temperature in the disk does not go below 10^3 K.

Computed variables for the SN-II model

Figure 7 shows the computed t_{ST} and t_{fade} for SNII. There is only a negligible difference in those computed values for SNIISFB (less than 2%). We also note that these variables are computed at the time of the SN-II feedback, and that they are

remembered by the kicked gas particle until it experiences the feedback again from other exploding stars nearby. Note that the gas density is always recalculated regardless of whether the gas is under the influence of the feedback or not.

From the figure we see that t_{ST} never exceeds 10^6 years and the typical duration of the ST phase is on the order of 10^4 to 10^5 years. Since the t_{ST} is equivalent to the time at which the radiative cooling starts to become non-negligible on the outer SNR shell, we conclude that the typically used value in literature for the artificial turning off of the cooling for a period of the order of 10^7 years is considered unphysical. We also note that our SN-II model is capable of producing outflows with the wind velocity reaching up to $\sim 200 \text{ km s}^{-1}$.

Resolution dependency

We test the model's dependency on the numerical resolution with isolated galaxies and compare the SF history for selected cases in Figure 8. The gravitational softening length is reduced from 80 to 30 pc for SNIISFB and to 25 pc for WINDS. The efficiency of the feedback in suppressing the SFR seems to be slightly compromised if the resolution is higher for both SNIISFB and WINDS. This is manifested in the early times, namely at the onset (and before $\sim 250 \text{ Myr}$) with the larger spiky SFR for SNIISFB due to the formation of dense gas regions where there is little young stars that can add feedback energy into the ISM. Nonetheless, there is a minor difference in the overall results, and both cases show a reasonably good convergence.

One of the possible reasons for the inefficient feedback effects seen in the higher resolution SNIISFB case presumably arises from the way the feedback energy is calculated. First, in the higher resolution case all the particles, including gas and stars, have an order of magnitude smaller mass – e.g. $M_\star \sim 10^3 M_\odot$, compared to that of the lower resolution case of $\sim 10^4 M_\odot$. As we calculate the available feedback energy by the IMF for each stellar population, the smaller mass simply means

less available feedback energy from a single stellar population for distribution to the IMS. The strength of the wind velocity and the size of the shock radius (Equations 2.3 & 2.4) are all dependent on the amount of the feedback energy, so that by design the effectiveness of the SNII and SFB might be compromised even with the increased number of particles for the higher resolution case.

For comparison, it is interesting to see that the suppression of the SFR by WINDmed becomes weaker at later times as opposed to SNIISFBmed (the suffix 'med' is for the higher resolution cases). The primary difference in WINDS and SNIISFB is the strength of the outflows; WINDS produces stronger outflows as seen in Figure 4. A plausible scenario as to why this is the case could come from the fact that the strength of the outflows is controlled by the SFR since they are more tightly coupled in the WINDS model. That is, as the SFR progressively declines due to the consumption of the gas on the disk, so does the outflow rates, which in turn makes the suppression of the SFR weaker at later times.

Figure 9 helps us understand better the effectiveness of the feedback by examining the phase diagram and the fractional gas mass distribution of low and higher resolutions at $t = 0.7$ Gyr. The hot gas fraction ($T > 10^5$ K) is entirely due to the thermal feedback from both SNII and SFB, and that the higher resolution case shows a smaller fraction of the hot gas. Meanwhile, the warm ($5000 < T < 10^5$ K) and cold gas ($T < 5000$ K) show slightly higher fractions in the higher resolution case. Unlike the hot gas, they are concentrated in the denser regions, having peaks around $\log n_{gas} = -1$ to 0, which makes those warm gas in the higher resolution case more susceptible to cooling (i.e. the larger density results in a shorter cooling time). Additionally, the left tail of the warm gas in the low resolution case is more extended to the less dense region, which implies the gas can remain as non-star-forming for a longer time after receiving the feedback energy, and thus the low resolution case suppresses the SFR slightly more efficiently.

CHAPTER 6

PRELIMINARY TEST RESULTS WITH COSMOLOGICAL ZOOM-IN SIMULATIONS

In this chapter we present preliminary results of our SN-II and SFB feedback models tested on cosmological zoom-in simulations. We specifically look at the stellar-to-halo mass ratio and compare with previous models. We acknowledge that the SPH Galaxy Reduction suite (SPHGR) written by Robert Thompson is used as an analysis tool to make Figure 11.

Setup

For our preliminary testing on cosmological zoom-in simulations, we use an IC from the *AGORA* project with a lower resolution. The IC is generated by the *MUSIC* code (Hahn & Abel, 2011) with $[\ell_{min}, \ell_{max}] = [7, 10]$ in a box length of $60h^{-1}$ comoving Mpc. It forms a galactic halo of virial mass $M_{vir} \simeq 1.7 \times 10^{11} M_{\odot}$ at $z = 0$ with a quiescent merger history (Kim et al., 2014). We adopt the following cosmological parameters: $\Omega_m = 0.272$, $\Omega_L = 0.728$, $\Omega_b = 0.0455$, $H_0 = 70.2$, $n_{spec} = 0.961$ and $\sigma_8 = 0.807$. The gravitational softening length is set at 586 pc for high resolution particles (gas, dark matter and stars) and at 1.172 kpc for low resolution particle (bulge).

Stellar-to-halo mass ratio

Figure 11 shows the stellar-to-halo mass ratio for the selected runs. In the figure, it is shown that SNIISFB successfully reproduces good agreement with the observational data (Behroozi et al., 2013). SNIISFB not only efficiently regulates the SFR at the lower-mass end, it also reproduces the observational trends better, while the other runs plateau by keeping a higher stellar mass ratio at the low-mass end. There seems to be, however, an inefficiency in suppressing the SFR at the lowest-mass end

even for SNIISFB.

Comparing SNII and WINDS, both closely follow a similar trend as naively expected from the fact that their SFRs tested on the isolated galaxy show a minor difference. The difference we saw in comparing their outflow rates for the isolated galaxy seems to be not affecting the stellar-to-halo mass ratio – the stronger outflows produced by WINDS virtually does not make a significant difference here. We highlight again that a more physically-based model of SN-II is capable of reproducing the identical stellar-to-halo mass ratio with WINDS which turns off hydrodynamical interactions by hand for the wind particles.

The number of galaxies also is affected by the feedback. The well-known *missing satellites problem* in which numerical galaxy formation simulations have been known to produce too many satellites for a MW-type galaxy compared to observations (Klypin et al., 1999; Moore et al., 1999). Figure 12 shows the gas density projection of SH03SF model and SNIISFB compared, and the missing satellites problem is clearly alleviated by the implementation of SN-II and SFB in combination. The missing satellites problem is tightly related to the overcooling problem; i.e. the small satellites are overproduced due to the overcooling problem where the cold gas is accreted more effectively because of the lack of pressure support from feedback such as SNe. Therefore, our SN-II feedback and SFB are effective enough to resolve the overcooling problem, and as a result it successfully alleviates the missing satellites problem.

CHAPTER 7

DISCUSSION & CONCLUSIONS

We have presented an improved version of SN-II model and tested with a phenomenological SFB model for galaxy formation simulations. The new model has been tested first on isolated galaxies to examine the sub-kpc behavior of the feedback effects, and then we have presented a preliminary result on the cosmological zoom-in simulations. The results appear to be promising on both isolated galaxies and cosmological zoom-in simulations as the new model proves to alleviate some of the well-known problems in galaxy formation simulations, such as overcooling problem and missing satellites problem *without* the need for artificial adjustments of turning off hydrodynamical interactions and star formation by hand for the model to reproduce our expected results. In our model, cooling is only turned off during the ST phase where the radiative cooling is negligible. We employed the ST solution to calculate the variables, i.e. the wind velocities, shock radius and the transition times for the four evolutionary phases of SNR, rather than using a fixed value that can be a function of some adjustable parameters.

The most crucial improvement in the new model is that it is a physically-motivated implementation of SN-II feedback. With the ST solution, the physical properties of SNR are calculated and assigned to the individual SPH particles instead of applying a constant value for all of them. This eliminates free parameters from the model, and thus the results are not purely controllable/adjustable by hand as however we might desire. The ST solution themselves are approximations; however, they can be reliably tested and used to modeling an SN-II feedback that captures the essential features of a part of the evolutionary stages of SNR.

Our key findings are:

- SNII or SFB alone is insufficient in reproducing good agreement with observations – the stellar-to-halo mass ratio shows our simulation results largely deviate

from observations unless SNII and SFB are combined. This conclusion is in agreement with the studies by Hopkins et al. (2013). SFB alone in particular shows enhanced SFR instead of suppressing it, especially at the earlier time. Its inefficiency in adding pressure support to the cold gas cloud leads to the formation of 'knots' of dense gas as seen in Figure 5 that is also commonly seen in SH03SF. Increasing ϵ_{SFB} from 10 to 30% helps regulating the SFR more strongly, while failing to resolve the dramatically increased early SFR (Figure 3). In contrast to SFB, SNII alone proves to be more effective and robust not only in regulating SFR but also in producing outflows. Kinetic feedback employed in SNII is clearly showing its advantage over a pure thermal feedback here. Even though tests on isolated galaxies show there is only a minor difference in SNII and SNIISFB, the improved robustness of SNIISFB over SNII is explicitly shown in the stellar-to-halo mass ratio from the cosmological zoom-in simulations.

- No artificial turning off of hydrodynamical interactions and star formation is necessary for our SNII+SFB model to achieve reasonable agreement with observations (e.g. stellar-to-halo mass ratio). The cooling is turned off only for the ST phase that is calculated by the ST solution with no free parameter associated with it. In other words, the application of the ST solution to approximate the physical evolution of the SNR can eliminate the necessity of the artificial adjustment and reduce the number of free parameters in order to raise the feedback efficiency *if* SNII is combined with SFB. The outflow can also be produced with the ST solution, although not as strong as WINDS. As the stellar-to-halo mass ratio shows, the production of strong outflows by WINDS is not necessarily the key factor in achieving agreement with observations. In fact, the addition of SFB to SN-II feedback seems to have a larger impact on the simulated galaxy properties on the cosmological zoom-in simulations. The possible reason for this is the larger simulation time-steps due to the coarse resolution compared to that of isolated galaxy simulations: they fluctuate

throughout the simulation time, but the difference can be an order of magnitude. The larger time-steps in cosmological zoom-in simulations deposit the stellar feedback energy in a larger fraction in a single time-step, achieving a stronger heating effect. This in turn implies a possible resolution dependency of SFB which would require further investigation.

- The ST solution used in the SN-II feedback for computing the variables shown in Figure 7 provides that the duration of the ST phase on average is \sim two orders of magnitude smaller than the duration applied for turning off cooling by hand in some SN models in literature. This is a strong implication that there are some missing ingredients in their models to achieve good agreement with observation.
- The preliminary results on the stellar-to-halo mass ratio shows that SNIISFB effectively reduces the stellar mass at the lower-mass end. The number of satellites in SNIISFB is also reduced compared to the other cases, providing an effective solution to the missing satellites problem (Figures 11 & 12). It is advisable to show the stellar mass function that quantifies the number of galaxies as a function of galaxy stellar mass. However, we would need to move forward and test our model on larger-scaled cosmological simulations to obtain larger samples to plot a reliable stellar mass function, which will be included in our future work.

Future work

We have presented yet another model of an SN-II feedback and studied the interplay between SN-II and SFB mainly on the isolated galaxies. Our preliminary results only give us a glimpse of how the new model behaves and affects the results on a cosmological zoom-in scale with a coarse resolution. The next step therefore has to be conducting more rigorous and extensive followup studies on cosmological scales with higher resolution and larger sampling to clarify the strengths and

weaknesses of our model.

Not only increasing the resolution and extending the size of the simulations, we would also need to test the model with a series of ICs that could either produce larger galaxies with galaxy mass ranges covering up to $\sim 10^{12} - 10^{13} M_{\odot}$ to see whether or not the stellar-to-halo mass ratio still shows reasonable agreement with observations. The cosmological zoom-in IC used in this work produces a $10^{11} M_{\odot}$ galaxy as the largest galaxy with quiescent merger history. Because galaxy mergers affect significantly the galaxy properties and their subsequent evolutions, it would be valuable to test and study how our new model alters the evolutionary processes on such a system with violent merger history.

Furthermore, it is certainly not adequate to only consider SN-II and SFB: SN-Ia and AGN should play a critical role in the overall feedback effects. In particular, AGN feedback has been widely studied in galaxy formation literature (e.g. Choi et al., 2014, 2013; Newton & Kay, 2013; Wagner et al., 2013) and believed to have energetically significant impacts on the galaxy properties indicated by observations (e.g. Schawinski et al., 2007; Zinn et al., 2013). Due to the larger energy budget with a typical luminosity of $10^{12} L_{\odot}$, AGN feedback could play a key role in matching the higher-mass end of the stellar-to-halo mass ratio from observations. Compared to the luminosity of typical supernovae, an AGN could have \sim two orders of magnitude larger energy budget: as such, it should never be overlooked. SN-Ia should certainly be in consideration, for the outcomes are generally not too dissimilar to that of SN-II, except for the delay time present in SN-Ia.

Aside from adding SN-Ia and AGN feedback, there is also a possibility of improvement by modifying the SFB and making it momentum-based that is powered by radiation pressure rather than pure thermal feedback. As we know from the notorious overcooling problem, thermal feedback is susceptible to cooling especially in star-forming regions, forcing some models used in literature to turn off

cooling by hand. In contrast, a momentum-based feedback preserves energy better without significantly being affected by cooling. The method has been studied and tested in literature and the results show its robustness in overall simulated galaxy properties without relying on artificially turning off cooling (e.g. Agertz et al., 2013; Aumer et al., 2013; Hopkins et al., 2011).

CHAPTER 8

AGORA COMPARISON PROJECT

In this section we summarize the studies on the dark matter-only high resolution simulations as a collaborating effort for the *AGORA* project (Kim et al., 2014). The project aims to scrutinize the discrepancies among a variety of galaxy formation simulation codes and methods in a systematic way. To facilitate the systematic analysis by a variety of participant groups, the project employs and implements a common set of physics and feedback prescriptions and analyzes the results with a common tool kit, *yt* (Turk & Smith, 2011). It is an on-going project that we have participated. (URL: <http://www.agorasimulations.org>)

The initial studies made by the project involve running a series of dark matter-only simulations with the same initial conditions prepared by the project to test any deviations that can be found among the codes. We as a UNLV group contributed to this test runs by providing the outputs and analyzed results to the project. We ran both a low-res and high-res dark matter-only simulations. Additionally, we also independently did a comparison study to see how each *GADGET* parameter affects the results for the low-res cases.

Simulation setup

We use the common initial conditions created by *MUSIC* to run and compare the dark matter-only simulations. The parameters used for *RUN1* and *RUN2* are summarized in Table 3. The mass resolution is $3.38 \times 10^5 M_{\odot}$ for *RUN1*, which contains 20,971,520 high resolution particles and 5,875,840 low resolution particles, whereas that of *RUN2* is $4.22 \times 10^4 M_{\odot}$, containing 167,772,160 high and 20,971,520 low resolution particles. In other words, both *RUN1* and *RUN2* are exactly the same except that *RUN2* has a higher resolution. We used *GADGET-3* for these runs.

Table 3 summarizes the tested runs for the *AGORA* project. For *RUN1*, we ex-

amined a series of cases with different options in the Makefile to see how each option affects the overall results. Moreover, for RUN1-A and RUN2, we set the softening length for comoving and physical differently in such a way that they are 'switched' to a finer one at $z = 9$ (i.e. the factor of 10 difference is from the $1 + z$ factor for the comoving frame). The detailed descriptions for the Makefile options can be found in the GADGET user guide by Volker Springel.

Overall results

The comparison between RUN1 and RUN2 shows a minor difference in the properties of the target halo. As shown in Table 3, the halo center, M_{vir} and R_{vir} all show a good convergence. The slightly large M_{vir} for RUN1-D is due to the presence of a subhalo within the target halo. In the meantime, the Makefile options listed in Table 3, which are primarily added to the code for improved computational techniques, do make a difference in the total CPU hours. The PMGRID option is clearly needed for faster computing time by comparing RUN1-A, B, C and RUN1-D. Furthermore, switching the softening length at $z = 9$ does reduce the computational expense, while the outcome remains unaffected (comparing RUN1-A and RUN1-B).

Density projection

Figure 13 compares the projected gas density at $z = 0$ for RUN2 and RUN1-A. The overall dark matter structure of both RUN1 and RUN2 are in good agreement. Although it may not be obvious from the Figure, the primary difference is that the overall filamentous structure of RUN2 seems to be more tightly packed (see animation at: <http://www.physics.unlv.edu/~keitee/AGORA/6Mpch.swf>). The possible reason would be that the increased number of particles for RUN2 creates stronger gravitational interactions between the particles. This in turn forms more subhalos for RUN2; for instance, a small subhalo is seen at the two o'clock direction on the

target halo only in the RUN2 1Mpc/h image.

Density profile

Figure 14 shows radially averaged density profiles of the target halo at $z = 0$. All the cases, except for RUN1-D, agree with each other remarkably well. The slight deviation seen in the case RUN1-D with a higher density at the outer radius is most likely due to the presence of a subhalo that is unique to RUN1-D. Figure 14 additionally includes the results from another GADGET code and an ENZO code, which show a general agreement with our code. The detailed results that compare with all the other participating codes are presented in Kim et al. (2014).

Discussion

In summary, the initial dark matter-only proof of concept runs show good agreement among all the codes with minimal resolution dependency. The primary difference seen among the codes are the locations of subhalos, which could slightly affect the density profiles. As for the next step, the *AGORA* project will examine the numerical convergence among the codes when gas is included with a common cooling and star formation routines and a set of feedback mechanisms. The strengths and weaknesses of each code will then be addressed in a systematic manner so that the forthcoming galaxy formation simulations can move forward to a new generation with an enhanced predictive power of galaxy formation.

Param Name	Symbol	Value
Disk mass	M_{disk}	$4.3 \times 10^{10} M_{\odot}$
Gas mass	M_{gas}	$8.6 \times 10^9 M_{\odot}$
R_{200} mass	M_{200}	$1.07 \times 10^{12} M_{\odot}$
Total mass	M_{tot}	$1.3 \times 10^{12} M_{\odot}$
R_{200}	R_{200}	205 kpc
Scale length	r_{disk}	3.43 kpc
Scale height	h_{disk}	0.343 kpc
Number of gas particle	N_{gas}	1×10^5
Number of dark matter particle	N_{DM}	1×10^5
Number of disk particle	N_{disk}	1×10^5
Number of bulge particle	N_{bulge}	1250
Gas particle mass	m_{gas}	$8.59 \times 10^4 M_{\odot}$
Dark matter particle mass	m_{DM}	$1.25 \times 10^7 M_{\odot}$
Disk particle mass	m_{disk}	$3.44 \times 10^5 M_{\odot}$
Bulge particle mass	m_{bulge}	$3.44 \times 10^5 M_{\odot}$
Softening length	for all particle types	80 pc

Table 1 Disk parameters of the common IC for the idealized isolated galaxy, used in the project *AGORA* (Kim et al., 2014). M is for the galaxy mass while m is for that of a single particle. r_{disk} is the scale length and h_{disk} is the scale height of the disk. Increasing the resolution from low to medium or from medium to high reduces m by a factor of 10, while it increases the total number of each particles by the same factor.

Label	Feedback	ϵ_{SFB}
SNII	SN-II	0
SNIISFB1	SN-II+SFB	0.1
SNIISFB2	SN-II+SFB	0.2
SNIISFB3	SN-II+SFB	0.3
SFB1	SFB	0.1
SFB2	SFB	0.2
SFB3	SFB	0.3

Table 2 Feedback efficiency parameters for tested cases. Note that the feedback efficiency only applies to the stellar feedback (SFB), where it ranges from 0.1 to 0.3 (10 to 30%). We use $\epsilon_{SFB} = 0.1$ as the fiducial (Stinson et al., 2013).

Labels	Softening length [kpc/h]	Total CPU hours	TreePM options	Halo center	M_{vir} [M_{\odot}]	R_{vir} [kpc]
RUN2	1.14 = comoving 0.114 = physical	39705	PMGRID=256 RCUT=4.5 PLACEHIGHRESREGION=2 ENLARGERECTION=1.2	(0.484631, 0.525307, 0.489904)	1.704e11	144.9
RUN1-A	3.22 = comoving 0.322 = physical	633	Same as RUN2	(0.486773, 0.525076, 0.491379)	1.675e11	144.3
RUN1-B0.322	= comoving = physical	806	Same as RUN2	(0.486766, 0.525132, 0.491333)	1.682e11	144.5
RUN1-C0.322	= comoving = physical	980	PMGRID=256	(0.486478, 0.525153, 0.491899)	1.661e11	143.9
RUN1-D0.322	= comoving = physical	5272	None	(0.484387, 0.525912, 0.492511)	1.728e11	145.6

Table 3 Parameters for dark matter-only *AGORA* simulations. Halo center, M_{vir} and R_{vir} of the target halo (the largest halo) are calculated values by a halo group finder *Rockstar* ver. 0.99.9 (Behroozi et al., 2013). The halo centers are given in (x,y,z)-coordinates.

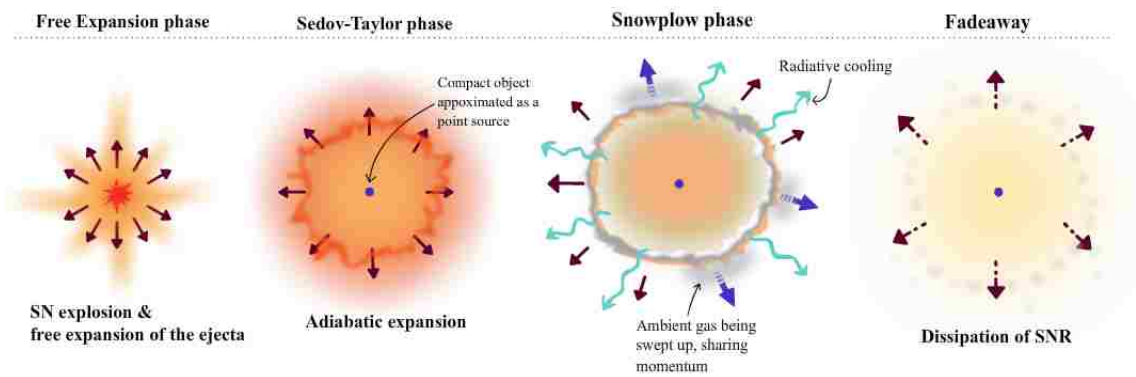


Figure 1 A schematic evolutionary phases of SNR. It starts out with a SN explosion immediately followed by a free expansion phase (left-most), then proceeds to the Sedov-Taylor phase with adiabatic expansion. The SNR forms a dense shell during the snowplow phase, and radiative cooling sets in before it dissipates into the surrounding medium.

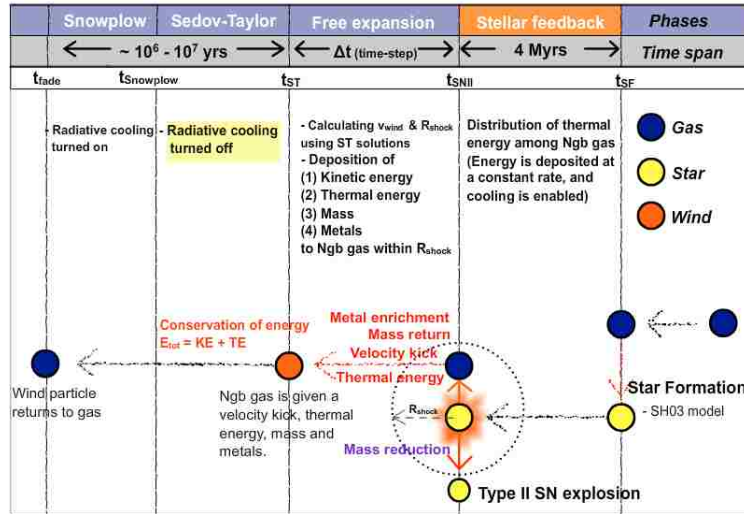


Figure 2 A schematic representation of the SN-II feedback model for the SPH code. *Star Formation*: An SPH (gas) particle first goes through star formation (SF), following a modified version of the SF recipe, originally from Springel & Hernquist (2003). A star particle is allowed to be born from a gas particle at each time-step if the gas density exceeds the SF threshold density. *Stellar feedback*: For the next 4 Myr the newly formed star particle continuously deposits thermal energy into the ambient gas medium at a constant rate. *Free Expansion*: The typical free expansion phase for a single stellar explosion only lasts a hundred to a thousand years. However, since a star particle in the SPH simulations is treated as a stellar population, the free expansion phase for a collection of stellar explosions lasts longer than a thousand years due to the accumulation effect. This becomes comparable to a single time-step that can be achieved by a high-resolution cosmological zoom-in (Hahn & Abel, 2011) or by an isolated galaxy simulations. Therefore, we treat one single time-step immediately after the stellar age reaches 4 Myr to be the free expansion phase in this model. During this phase, the total SNe energy available from a star particle is calculated by a Chabrier (2003) IMF and it is used to further calculate the followings: (1) the total kinetic energy (~ 28%) that is converted to the wind velocity and given to the neighboring gas particles in a form of velocity kick (2) the total thermal energy (~ 72%; Durier & Dalla Vecchia 2012) that is deposited in the neighboring gas particles (3) the time t_{ST} , $t_{Snowplow}$, and t_{fade} based on the ambient gas density and the total SN energy (4) the shock radius (R_{shock}) that is used to find the number of neighboring gas particles to be influenced by the SN-II feedback (5) the mass loss by the exploding star particle, and the mass return to the neighboring gas (6) metal production (Fe & O) by the exploding star particle and its distribution among the neighboring gas. Both (5) and (6) are computed based on the criteria described by Kim et al. (2014). *Sedov-Taylor Phase*: The wind particle travels by itself and produces galactic outflows until $t = t_{Snowplow}$. Radiative cooling is turned off during this phase to mimic its adiabatically expanding nature.

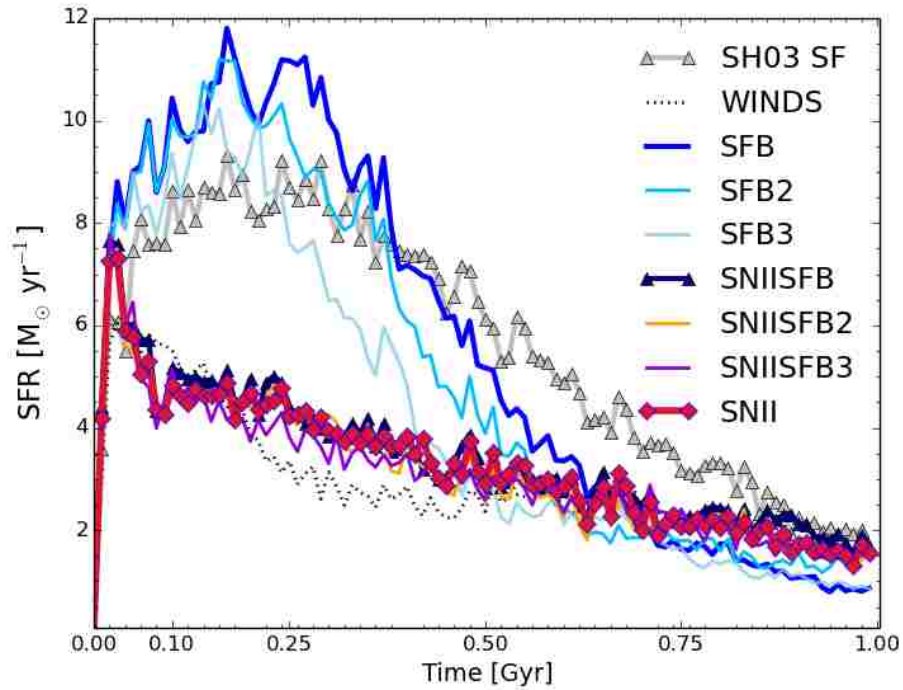


Figure 3 Star formation history of the tested cases for the isolated galaxy simulations compared. SH03SF is the star formation model described by Springel & Hernquist (2003) which incorporates the previous phenomenological SN model. WINDS adds a kinetic feedback to SH03SF so that it produces bipolar outflows of which the model is also described in Springel & Hernquist (2003). The other labels are summarized in Table 2.

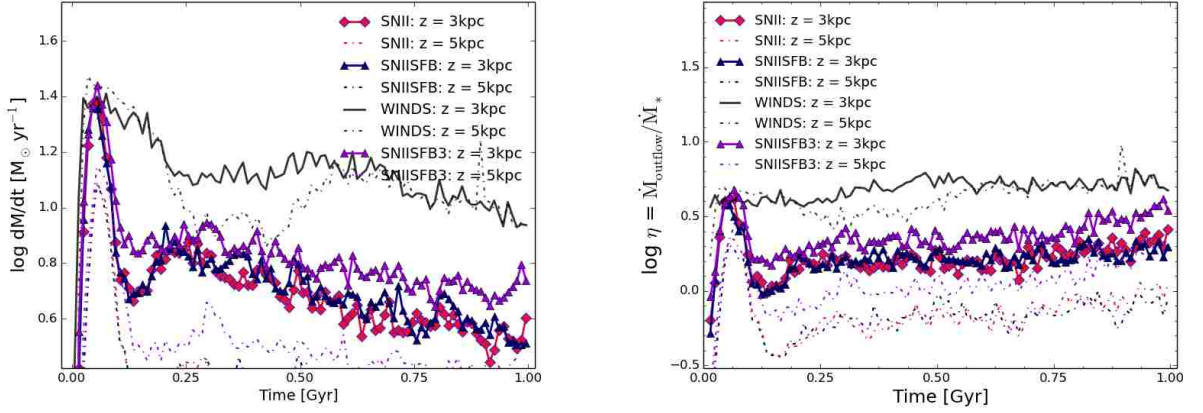


Figure 4 Outflow rates (dM/dt) and mass loading efficiency (η) compared. The compared cases are SN-II only (SNII), both SN-II and stellar feedback (SNIISFB), WINDS and SNIISFB with the $\epsilon_{SFB} = 0.3$ (SNIISFB3). *Left*: The outflow rate is calculated at the z -plane 3 & 5 kpc away from the disk center, showing the total outflow rate, which is the sum of the outflow rates above and below the disk center. *Right*: $\bar{\eta}$ is the mean value of η , averaged over the entire runtime (= 1 Gyr).

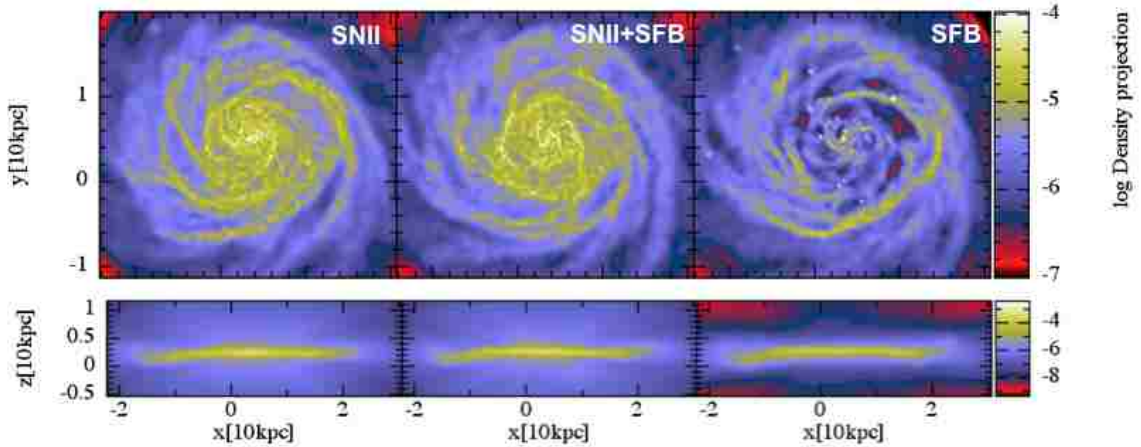


Figure 5 Projected gas density for the isolated disk galaxy simulations. The snapshot is at $t = 1$ Gyr. SFB alone creates large low-density regions in the inner disk due to the intense consumption of the gas that is converted to stars. A nearly identical result is also seen for SH03SF alone case (not shown). Meanwhile, SNII prevents the formation of the knots seen in SFB (or SH03SF) and produces more sturdy and distinctive spirals.

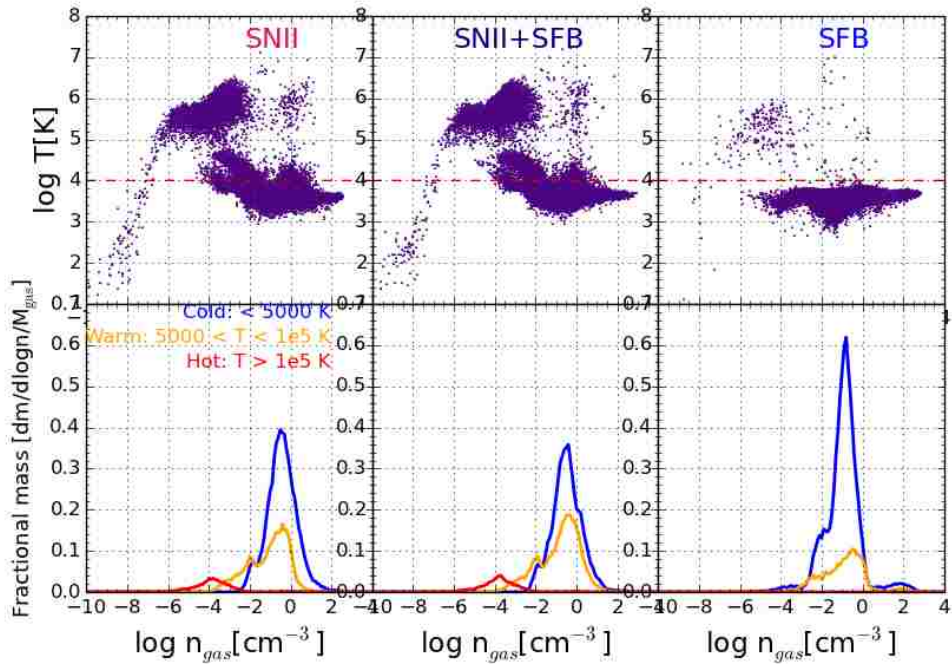


Figure 6 Temperature variations in the gas mass for the isolated galaxy simulations at $t = 1$ Gyr. The gas particles affected by the feedback increase their internal energy and rise up in the phase diagram (top panel). Those that escape the galaxy potential become outflows and cool adiabatically, moving toward bottom-left as seen in the tail.

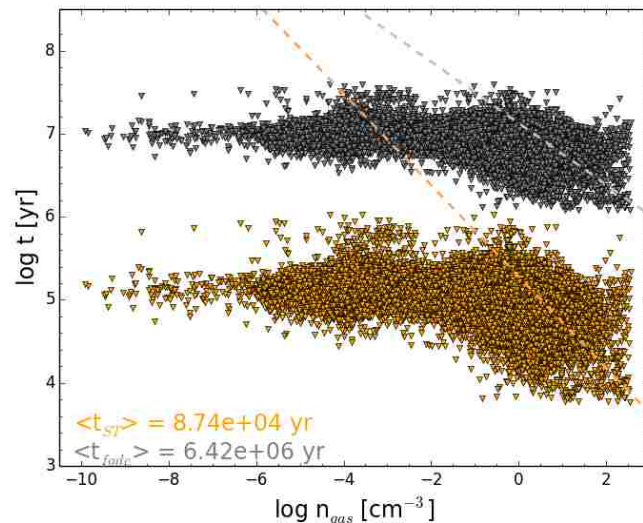


Figure 7 Computed variables for SNII feedback. The variables are the time of the end of the ST phase and fadeaway for each gas particle in the isolated galaxy simulations. The dashed lines are the typical values with a fixed SN energy available for the feedback.

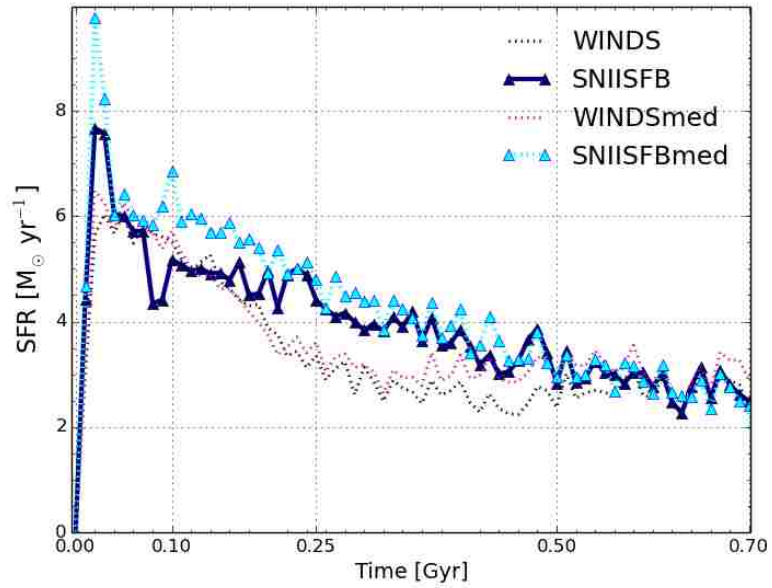


Figure 8 Resolution dependency test: star formation histories. The compared star formation histories are low and higher resolutions with the spatial resolutions of 80 and 30 pc, respectively. The legends suffixed with 'med' are the higher resolution cases.

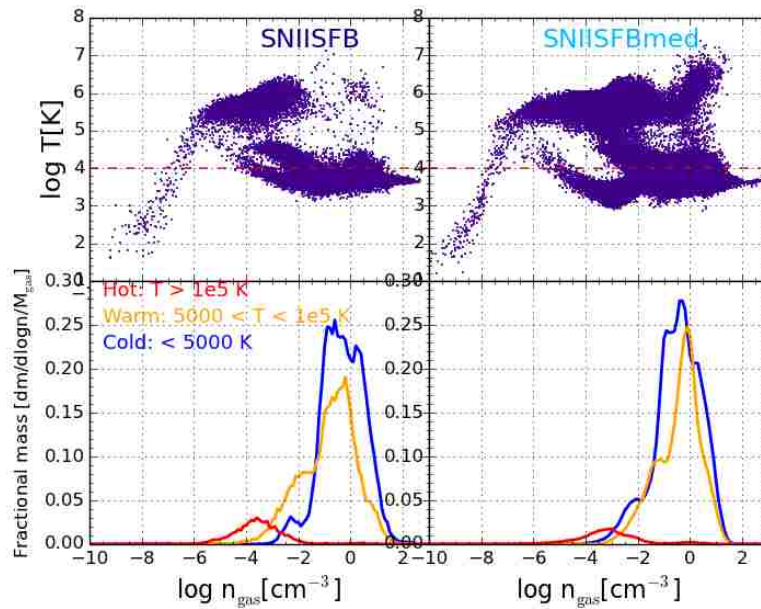


Figure 9 Resolution dependency test: phase diagram & fractional gas mass.

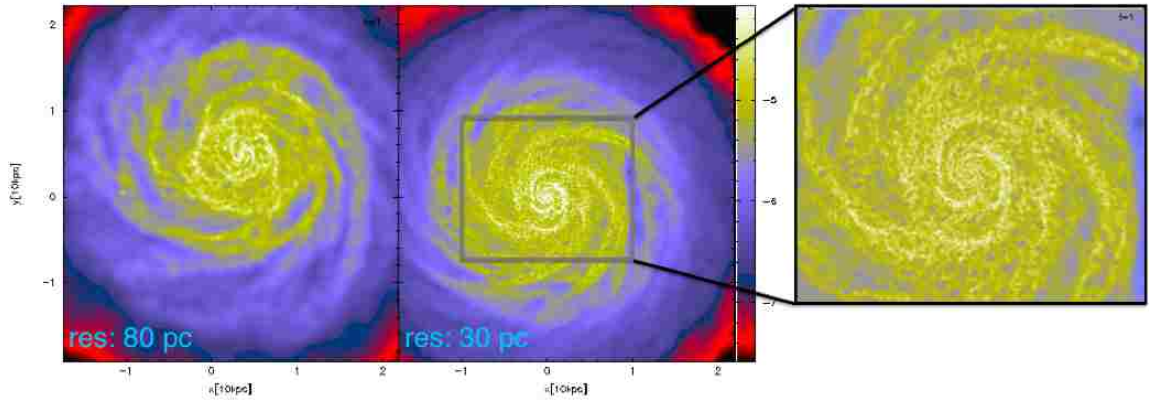


Figure 10 Resolution dependency test: visualization. The gas density projections of SNIISFB with resolutions of 80 and 30 pc are compared. The finer resolution case captures the formation of hot low-density 'bubbles' produced by the SN-II feedback more explicitly. Note that the finer resolution is accompanied with a larger number of particles in the simulations (see the caption of Table 1).

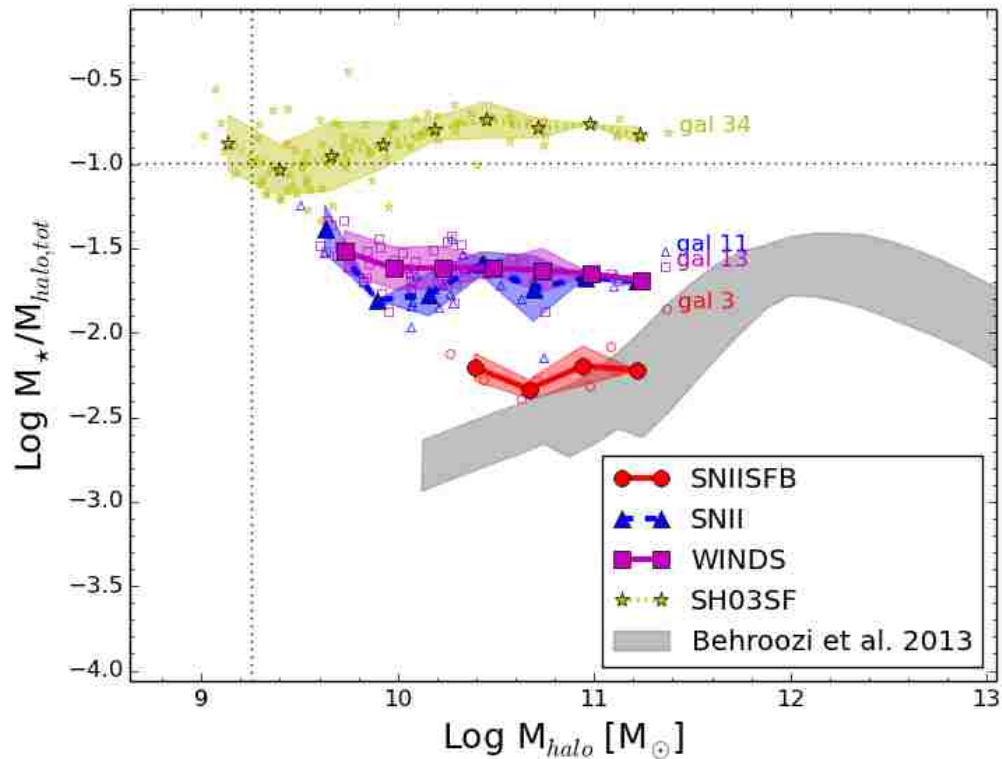


Figure 11 Stellar-to-halo mass ratio compared for the cosmological zoom-in simulations at $z = 0$. The labels are assigned for the largest galaxy in each simulation and the number associated with it is simply the galaxy ID.

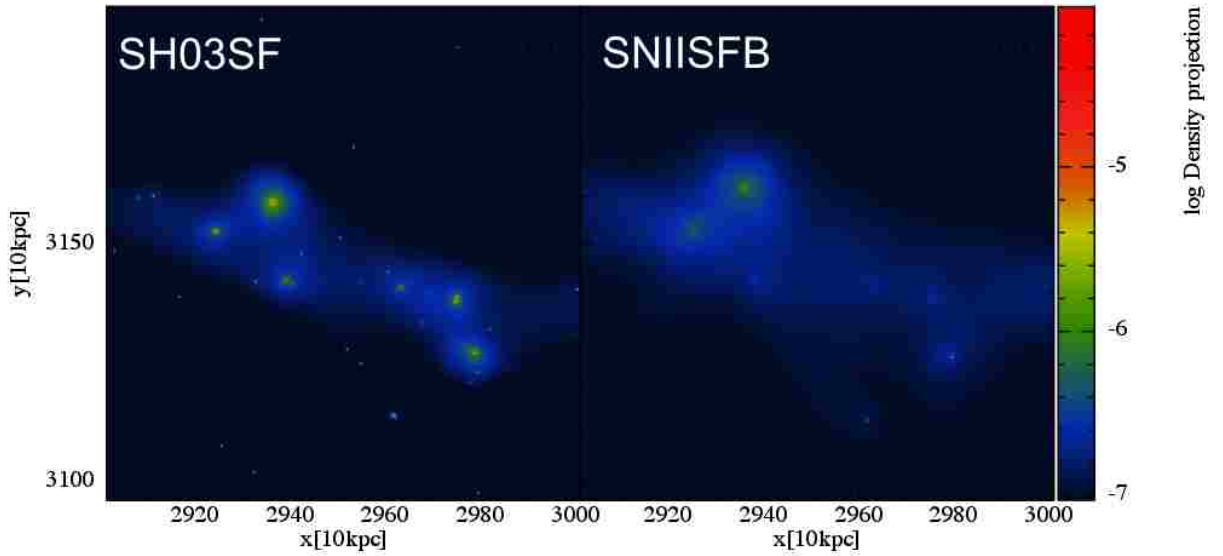


Figure 12 Projected gas density in $L = 1 \text{ Mpc}/h$ for the zoom-in simulations at $z = 0$. The gas distribution is more diffusive and the number of satellite galaxies is significantly reduced by the feedback effect for SNIISFB.

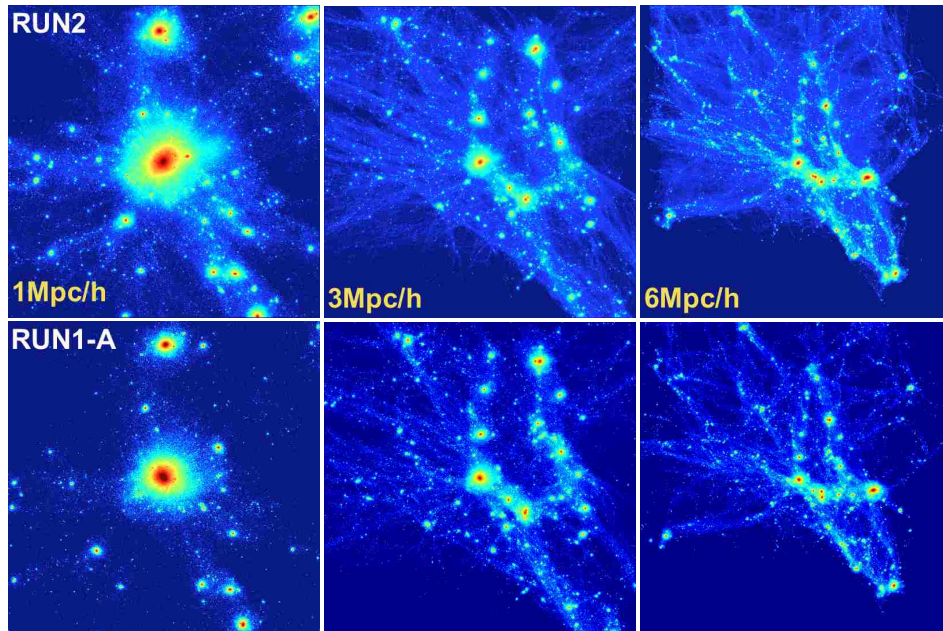


Figure 13 Projected dark matter density at $z = 0$. The presented cases are RUN2 and RUN1-A within a $1, 3$ and $6 \text{ Mpc } h^{-1}$ box centered on the target halo.

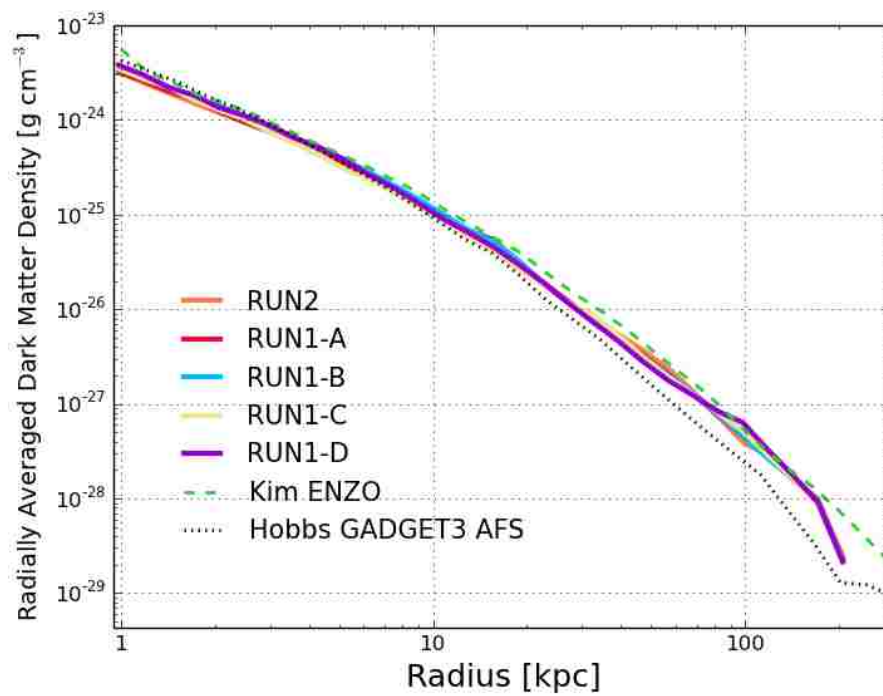


Figure 14 Dark matter density profiles of the target halo at $z = 0$. For comparison, the profiles provided by Ji-hoon Kim (ENZO) and Alex Hobbs (GADGET-3 AFS) are also shown.

REFERENCES

- Agertz, O., Kravtsov, A. V., Leitner, S. N., & Gnedin, N. Y. 2013, *ApJ*, 770, 25
- Aumer, M., White, S. D. M., Naab, T., & Scannapieco, C. 2013, *MNRAS*, 434, 3142
- Balogh, M. L., Pearce, F. R., Bower, R. G., & Kay, S. T. 2001, *MNRAS*, 326, 1228
- Behroozi, P. S., Wechsler, R. H., & Conroy, C. 2013, *ApJL*, 762, L31
- Burrows, A. 2013, *Reviews of Modern Physics*, 85, 245
- Burrows, A., Reddy, S., & Thompson, T. A. 2006, *Nuclear Physics A*, 777, 356
- Chabrier, G. 2003, *ApJL*, 586, L133
- Choi, E., Ostriker, J. P., Naab, T., Oser, L., & Moster, B. P. 2014, *ArXiv e-prints*
- Choi, J. H. & Nagamine, K. 2009, *MNRAS*, 393, 1595
- . 2011, *MNRAS*, 410, 2579
- Choi, J.-H., Shlosman, I., & Begelman, M. C. 2013, *ApJ*, 774, 149
- Cox, D. P. 1972, *ApJ*, 178, 159
- . 1993, *Astronomical Society of the Pacific Conference Series*, Vol. 35, *Late Stages in Supernova Remnant Evolution*, ed. J. P. Cassinelli & E. B. Churchwell, 402
- Dalla Vecchia, C. & Schaye, J. 2008, *MNRAS*, 387, 1431
- . 2012, *MNRAS*, 426, 140
- Draine, B. T. 2011, *Physics of the Interstellar and Intergalactic Medium* (New Jersey: Princeton University Press)
- Dubois, Y. & Teyssier, R. 2008, *A&A*, 477, 79
- Durier, F. & Dalla Vecchia, C. 2012, *MNRAS*, 419, 465
- Haardt, F. & Madau, P. 1996, *ApJ*, 461, 20
- Hahn, O. & Abel, T. 2011, *MNRAS*, 415, 2101
- Hanasz, M., Lesch, H., Naab, T., Gawryszczak, A., Kowalik, K., & Wóltański, D. 2013, eprint arXiv:1310.3273
- Haxton, W. C. 2000, in *Neutrinos in Physics and Astrophysics*, ed. P. Langacker, 432–487
- Hopkins, P. F. 2013, *MNRAS*, 428, 2840

- Hopkins, P. F., Keres, D., Onorbe, J., Faucher-Giguere, C.-A., Quataert, E., Murray, N., & Bullock, J. S. 2013, ArXiv e-prints
- Hopkins, P. F., Quataert, E., & Murray, N. 2011, MNRAS, 417, 950
- Katz, N., Weinberg, D. H., & Hernquist, L. 1996, ApJS, 105, 19
- Kay, S. T., Pearce, F. R., Frenk, C. S., & Jenkins, A. 2002, MNRAS, 330, 113
- Kereš, D., Katz, N., Davé, R., Fardal, M., & Weinberg, D. H. 2009, MNRAS, 396, 2332
- Kim, J.-h., Abel, T., Agertz, O., Bryan, G. L., Ceverino, D., Christensen, C., Conroy, C., Dekel, A., Gnedin, N. Y., Goldbaum, N. J., Guedes, J., Hahn, O., Hobbs, A., Hopkins, P. F., Hummels, C. B., Iannuzzi, F., Keres, D., Klypin, A., Kravtsov, A. V., Krumholz, M. R., Kuhlen, M., Leitner, S. N., Madau, P., Mayer, L., Moody, C. E., Nagamine, K., Norman, M. L., Onorbe, J., O'Shea, B. W., Pillepich, A., Primack, J. R., Quinn, T., Read, J. I., Robertson, B. E., Rocha, M., Rudd, D. H., Shen, S., Smith, B. D., Szalay, A. S., Teyssier, R., Thompson, R., Todoroki, K., Turk, M. J., Wadsley, J. W., Wise, J. H., Zolotov, A., & AGORA Collaboration 2014, ApJS, 210, 14
- Klypin, A., Kravtsov, A. V., Valenzuela, O., & Prada, F. 1999, ApJ, 522, 82
- Lopez, L. A., Castro, D., Slane, P. O., & Ramirez-Ruiz, E. 2013, ArXiv e-prints
- Moore, B., Ghigna, S., Governato, F., Lake, G., Quinn, T., Stadel, J., & Tozzi, P. 1999, ApJL, 524, L19
- Morris, J. P. 1996, Pub. Astr. Soc. Aust., 13, 97
- Newton, R. D. A. & Kay, S. T. 2013, MNRAS, 434, 3606
- Oppenheimer, B. D. & Davé, R. 2006, MNRAS, 373, 1265
- Osterbrock, D. E. & Ferland, G. J. 2006, Astrophysics of gaseous nebulae and active galactic nuclei
- Rest, A., Foley, R. J., Gezari, S., Narayan, G., Draine, B., Olsen, K., Huber, M. E., Matheson, T., Garg, A., Welch, D. L., Becker, A. C., Challis, P., Clocchiatti, A., Cook, K. H., Damke, G., Meixner, M., Miknaitis, G., Minniti, D., Morelli, L., Nikolaev, S., Pignata, G., Prieto, J. L., Smith, R. C., Stubbs, C., Suntzeff, N. B., Walker, A. R., Wood-Vasey, W. M., Zenteno, A., Wyrzykowski, L., Udalski, A., Szymański, M. K., Kubiak, M., Pietrzyński, G., Soszyński, I., Szewczyk, O., Ulaczyk, K., & Poleski, R. 2011, ApJ, 729, 88
- Saitoh, T. R. & Makino, J. 2009, ApJL, 697, L99
- . 2013, ApJ, 768, 44

- Schawinski, K., Thomas, D., Sarzi, M., Maraston, C., Kaviraj, S., Joo, S.-J., Yi, S. K., & Silk, J. 2007, *MNRAS*, 382, 1415
- Sedov, L. I. 1959, *Similarity and Dimensional Methods in Mechanics* (New York: Academic Press)
- Shu, F. H. 1992, *The Physics of Astrophysics Volume II Gas Dynamics* (California: University Science Books)
- Silk, J., Di Cintio, A., & Dvorkin, I. 2013, ArXiv e-prints
- Springel, V. 2005, *MNRAS*, 364, 1105
- Springel, V., Frenk, C. S., & White, S. D. M. 2006, *Nature*, 440, 1137
- Springel, V. & Hernquist, L. 2003, *MNRAS*, 339, 289
- Stinson, G., Seth, A., Katz, N., Wadsley, J., Governato, F., & Quinn, T. 2006, *MNRAS*, 373, 1074
- Stinson, G. S., Brook, C., Macciò, A. V., Wadsley, J., Quinn, T. R., & Couchman, H. M. P. 2013, *MNRAS*, 428, 129
- Taylor, G. 1950, *Royal Society of London Proceedings Series A*, 201, 159
- Turk, M. J. & Smith, B. D. 2011, ArXiv e-prints
- Wagner, A. Y., Umemura, M., & Bicknell, G. V. 2013, *ApJL*, 763, L18
- Weinberg, D. H., Hernquist, L., & Katz, N. 2002, *ApJ*, 571, 15
- White, S. D. M. & Frenk, C. S. 1991, *ApJ*, 379, 52
- Woosley, S. & Janka, T. 2005, *Nature Physics*, 1, 147
- Zinn, P.-C., Middelberg, E., Norris, R. P., & Dettmar, R.-J. 2013, *ApJ*, 774, 66

CURRICULUM VITAE

Graduate College
University of Nevada, Las Vegas

Keita Todoroki

Email: keitee@physics.unlv.edu

Web: <http://www.physics.unlv.edu/~keitee>

Education

Bachelor of Arts in Physics, December 2011
University of Hawai'i at Manoa. Honolulu, HI.

Biological Sciences (2006 - 2008)
Grossmont College. El Cajon, CA.

English as a Second Language (2005)
NIC International College in Japan. Tokyo, Japan.

Teaching Experience

Introductory Astronomy Lab (Fall 2012 - Spring 2014) at UNLV
General Physics Lab I (Fall 2012 & Summer 2013) at UNLV
Grader & Tutor for undergraduate physics (Spring & Summer 2012) at UNLV
Grader & Tutor for undergraduate physics (2011) at UH Manoa

Research

Adviser: Dr. Kentaro Nagamine (January 2012 - August 2014) at UNLV

Cosmological & isolated disk galaxy hydrodynamical simulations for galaxy formation

- Implementing and testing a Type II supernova and stellar feedback in a SPH code GADGET-3

Contributing to the *AGORA* comparison project on dark matter-only high resolution simulations

Co-authored Publication

The AGORA High – resolution Galaxy Simulations Comparison Project
Kim, J.-h. et al. *ApJS*, 210, 14.

Computational Skills

Programming experience in C, C++ and Python

Familiarity with UNIX and Microsoft Windows operating systems

Proficient in Microsoft Office and L^AT_EX software packages

Experience with numerical hydrodynamics, using and modifying SPH codes (GADGET-3)

Experience with high-performance parallel computing, on distributed memory (MPI) platforms

Experience with a SPH visualization software (SPLASH)

Workshop Attended

A mini-workshop at the Osaka University (March 9 - March 15, 2014)

The *AGORA* second workshop at the University of California, Santa Cruz (August 16 - 18, 2013)